NANO LETTERS

Letter

pubs.acs.org/NanoLett

# Enhanced Third-Harmonic Generation in Silicon Nanoparticles Driven by Magnetic Response

Maxim R. Shcherbakov,*[,†] Dragomir N. Neshev,[‡] Ben Hopkins,[‡] Alexander S. Shorokhov,[†] Isabelle Staude,[‡] Elizaveta V. Melik-Gaykazyan,[†] Manuel Decker,[‡] Alexander A. Ezhov,[†] Andrey E. Miroshnichenko,[‡] Igal Brener,[¶] Andrey A. Fedyanin,[†] and Yuri S. Kivshar[‡]

[†]Faculty of Physics, Lomonosov Moscow State University, Moscow 119991, Russia

[‡]Nonlinear Physics Centre, Research School of Physics and Engineering, The Australian National University, Canberra, Australian Capital Territory 0200, Australia

[¶]Center for Integrated Nanotechnologies, Sandia National Laboratories, Albuquerque, New Mexico 87185, United States

*S* *Supporting Information*

**ABSTRACT:** We observe enhanced third-harmonic generation from silicon nanodisks exhibiting both electric and magnetic dipolar resonances. Experimental characterization of the nonlinear optical response through third-harmonic microscopy and spectroscopy reveals that the third-harmonic generation is significantly enhanced in the vicinity of the magnetic dipole resonances. The field localization at the magnetic resonance results in two orders of magnitude enhancement of the harmonic intensity with respect to unstructured bulk silicon with the conversion efficiency limited only by the two-photon absorption in the substrate.

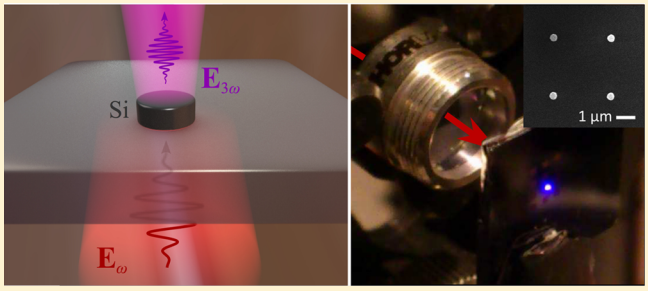


**KEYWORDS:** *nonlinear optics, third-harmonic generation, silicon nanoparticles, optical magnetism, multipole decomposition*

Nonlinear optics describes processes in which photons with new frequencies are coherently generated when light passes through an optical medium. The commonly known examples of such nonlinear processes are *doubling* and *tripling* the input frequency of light with a nonlinear crystal, when it is illuminated with an intense light field.[1] The optical properties of nanoscale structures differ substantially from bulk materials because they are affected by strong confinement resulting in geometrical resonances. For example, at the frequency of the localized plasmon resonances there is a strong enhancement of local electric fields with the formation of "hot spots", which are known to boost substantially nonlinear optical effects in metal nanostructures.[2] However, the strong local field enhancement in plasmonic systems comes only in a confined volume, which inevitably limits the nonlinear conversion efficiency. In contrast, resonances of high-index dielectric nanoparticles provide mode volume, which is not limited to interfaces, and despite the weaker field enhancement, the overall conversion efficiency is expected to be much higher.

As the second-harmonic generation is an even-order nonlinear process, it can be observed only for noncentrosymmetric structures. The third-harmonic generation (THG) process is a more general effect[3] because the symmetry-induced selection rules are more relaxed for the most of the known media. The first observation of the third-harmonic signal from single plasmonic nanoparticles was reported for gold colloids, and it was suggested for single-biomolecule tracking microscopy.[4] Many subsequent studies of the THG process have been conducted for metallic nanostructures such as plasmonic nanoantennas,[5,6] complex plasmonic Fano structures,[7] and plasmonic metamaterials.[8−10] However, nonlinear effects in resonant high-permittivity dielectric nanoparticles have not been reported. The importance of both electric and magnetic dipolar resonances on the nonlinear conversion efficiency in such particles still remains unknown.

Generally, high-permittivity nanoparticles are emerging as a promising alternative to metallic nanoparticles for a wide range of nanophotonic applications that utilize *localized resonant modes*, recently observed experimentally in the entire visible and near-IR spectral ranges in silicon nanospheres.[11,12] Such nanoparticles offer unique opportunities for the study of nonlinear effects due to very low losses in combination with multipolar characteristics of both electric and magnetic resonant optical modes. More importantly, the nonlinear optical effects of magnetic origin can have fundamentally different properties compared with those of electric origin. When nonlinearities of both electric and magnetic origin are present, the nonlinear response can be modified substantially being accompanied by nonlinear mode mixing and magneto-electric coupling studied so far only at microwave frequen-

**Received:** August 6, 2014
**Revised:** October 10, 2014
**Published:** October 16, 2014

   dx.doi.org/10.1021/nl503029j | *Nano Lett.* 2014, 14, 6488−6492

cies.[13,14] It is, therefore, an important task to characterize the optical nonlinear effects originating from the magnetoelectric response of high-index nanostructures. Furthermore, silicon is a material with high third-order nonlinearity; hence, strong enhancement can be expected in the nonlinear optical response of high-index nanoparticles.

In this Letter, for the first time to our knowledge, we study the nonlinear response from individual silicon disk nanoparticles in the vicinity of the magnetic resonance. We demonstrate that by engineering the resonant modes of such nanoparticles, we can control the locally enhanced electromagnetic fields, giving rise to two orders of magnitude enhancement of THG with respect to bulk silicon. The maximum IR-to-visible conversion efficiency is found to be limited only by the two-photon absorption process in the substrate.

For nonlinear optical studies of silicon nanoparticles, we make use of the nanodisk geometry. Silicon nanodisks have recently shown versatility in independent tailoring of electric and magnetic response stemming from two degrees of freedom: radius and height.[15] Also, as opposed to nanospheres, the fabrication of nanodisks is easily accessed by modern electron-beam lithography, which enables a precise control of the nanodisk size and lattice geometries. In our experiment, we address silicon nanodisks placed on silica as shown in Figure 1.

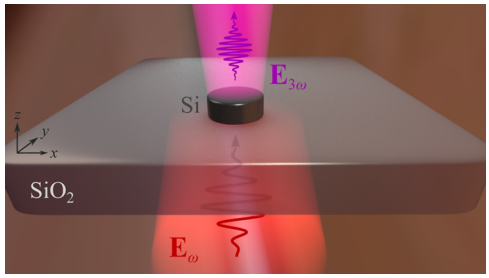


**Figure 1.** Illustration of THG from individual Si nanodisks at the magnetic dipole responance at optical frequencies. Each sample comprises a square array of silicon nanodisks on a 2-$\mu$m-thick $SiO_2$ layer situated on a bulk silicon substrate (not shown). Two sets of nanodisk arrays are considered: one with a disk diameter of $d$ = 360 nm, a height of $h$ = 260 nm, and a period of $p$ = 2.85 $\mu$m and the other one with $d$ = 500 nm, $h$ = 220 nm, and $p$ = 0.8 $\mu$m.

The disks are illuminated by an intense femtosecond laser pulse train with the frequency $\omega$ close to the magnetic dipole resonance of the former. As a result of the high silicon third-order susceptibility $\chi^{(3)}$, the transmitted signal contains pulses of the tripled fundamental frequency $3\omega$. Because the third harmonic (TH) signal is proportional to the local field intensity cubed, it is reasonable to anticipate considerable enhancement of the TH process in the nanodisks with their magnetic resonances excited by the fundamental wave.

Silicon nanodisks were fabricated via electron-beam lithography on backside polished (001)-cut silicon-on-insulator (SOI) wafers (SOITEC). The process was followed by a reactive-ion etching process using the obtained electron-beam resist pattern as an etch mask. Two square arrays of nanodisks with different nanodisk densities were fabricated: one with a period of 2.85 $\mu$m, intended for THG microscopy measurements, and the other with a period of 0.8 $\mu$m, intended for THG spectroscopy measurements.

A scanning electron micrograph of the first nanodisk array is shown in Figure 2a. Figure 2b shows the negative logarithm of the transmission spectrum obtained for this sample using a setup based on a white light source and an IR spectrometer (see Supporting Information, Section I). The spectrum is normalized over the spectrum of the adjacent sample area where the top Si layer is etched away.

Two resonances are seen in the spectrum. The shorter wavelength resonance is the electric dipole resonance of a single disk, and the longer wavelength resonance is the magnetic dipole resonance. This is determined by conducting full-wave simulations with CST Microwave Studio and performing a subsequent multipole expansion of the scattered field.[16] In Figure 2c the scattering cross-section of a single silicon nanodisk is decomposed to electric and magnetic dipole contributions exhibiting two distinct resonances. The false-color plots in Figure 2 provide the maps of the local fields excited within the disks at the electric and magnetic dipolar resonances. It is worth noting that the maximum local field value within the disk at the magnetic resonance is twice as large as the maximum field excited at the electric one. The discrepancy between the experimental and calculated positions of the electric dipolar resonance is likely due to several factors, including the presence of the substrate, deviations from a perfect disk shape due to not perfectly vertical nanodisk sidewalls realized in experiment[17] and the sensitivity of the electric resonance position to the nanodisk spacing. None of

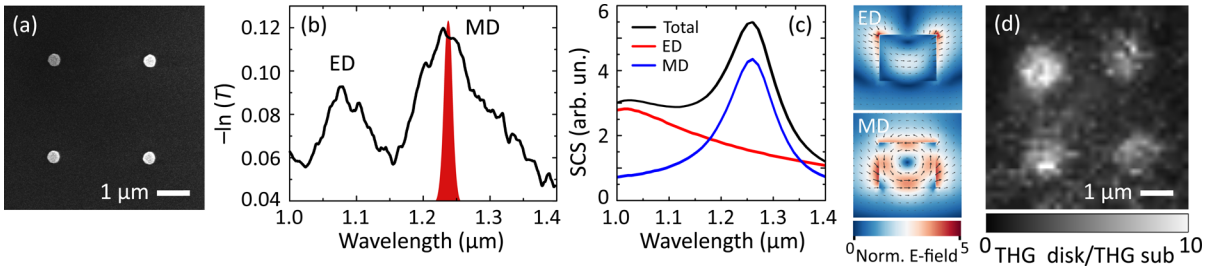


**Figure 2.** Spatially resolved THG from individual Si nanodisks enhanced by the magnetic resonance. (a) Scanning electronic microscopy image of an array of silicon nanodisks with $d$ = 360 nm, $h$ = 260 nm, and $p$ = 2.85 $\mu$m. (b) Experimental normalized transmission spectrum of the sample (black) with the pump pulse spectrum denoted with the red area. ED denotes the position of the electric dipole resonance, and MD shows the position of the magnetic dipole resonance. (c) Calculated scattering cross section (SCS) spectra of the nanodisks (black) decomposed to electric dipole (red) and magnetic dipole (blue) contributions with corresponding electric field distributions. (d) Microscopic image of the sample taken with a scanning optical microscope by detecting THG signal at $\lambda$ = 413 ± 5 nm. The signal is normalized by the signal acquired under the same conditions from the substrate area. Local-field-enhanced THG is seen at the nanodisk sites as compared to the substrate between them.


dx.doi.org/10.1021/nl503029j | Nano Lett. 2014, 14, 6488−6492

the mentioned factors are taken into account in Figure 2; the role of the lattice spacing is discussed in Supporting Information, Section VI.

In order to straightforwardly indicate the enhanced nonlinear response from single nanodisks, we perform THG microscopy and laser scanning microscopy using a confocal microscope and an external femtosecond optical parametric oscillator as a pump (see Supporting Information, Section II). Figure 2d shows an image of the first nanodisk array taken in the regime of the THG signal detection by tuning the spectrometer to the region of the TH radiation detection at 413 nm. Here, the pump radiation centered at $\lambda_{pump}$ = 1.24 $\mu$m is focused to a spot of approximately 5 $\mu$m in diameter to specifically address the magnetic dipole resonance of four nanodisks. THG is seen to be enhanced by a factor of up to 10 at the nanodisk sites if compared to THG from the bulk substrate in between them, despite that the substrate contains a silicon slab which is roughly 0.5 mm thick.

To further investigate the role of the magnetic resonance in the enhanced nonlinear response of the nanodisks, we perform THG spectroscopy measurements. Bulk silicon possesses a high intrinsic third-order nonlinear susceptibility of up to $\chi^{(3)}$ = 2.5 × $10^{-10}$ $esu^3$ as well as significant $\chi^{(3)}$ dispersion in the spectral range of interest caused by the resonant coherent three-photon direct transitions at $3\hbar\omega$ = 3.45 eV. To unambiguously disclose wavelength-dependent contributions coming specifically from the nanodisks and their magnetic dipole resonances, for each pump wavelength, THG was measured consecutively from the nanodisk arrays and from the adjacent area where the top silicon layer was etched away. Because the source of both TH signals is bulk silicon, normalizing THG from the samples by THG from the unstructured area cancels out the $\chi^{(3)}(\lambda)$ dispersion.

The relative density of the disks is very important for higher yield of the TH radiation. Therefore, we measure the THG spectra for the nanodisk array with a smaller period of $p$ = 0.8 $\mu$m. Also, we match the thickness of the disks to the penetration depth of the TH radiation into Si at the magnetic dipole resonance for better extraction of the TH from the whole nanodisk volume (see Supporting Information, Section V). As indicated with the gray area in Figure 3a, the sample possesses a resonance at 1.24 $\mu$m with considerable magnetic dipole component as indicated in Figure 3b. The resonance is characterized by enhanced local electric fields tightly bound within the nanodisk volume. Because the third-order nonlinear polarization scales with the local fields cubed, one expects a considerable enhancement of the nonlinear optical effects, including THG, from the disks pumped by the resonant laser radiation. This is proved by the THG spectrum of the sample shown with purple dots. We observe the resonance of the nanodisks enhance the THG by the factor of up to 100 as compared to the bulk silicon slab at the fundamental wavelength of $\lambda$ = 1.26 $\mu$m. This generates the 420 nm radiation bright enough to be observed by naked eye under the table-lamp illumination conditions as shown in the inset of Figure 4.

The THG resonance is seen to be split into two. The splitting can be connected to the microscopic structure of the fields within the disks and their multipole moments. Figure 3b shows the simulated transmission of the fundamental frequency through the disk array and substrate. This simulated transmission is in good agreement with that measured in the experiment. We extract the electric and magnetic dipole

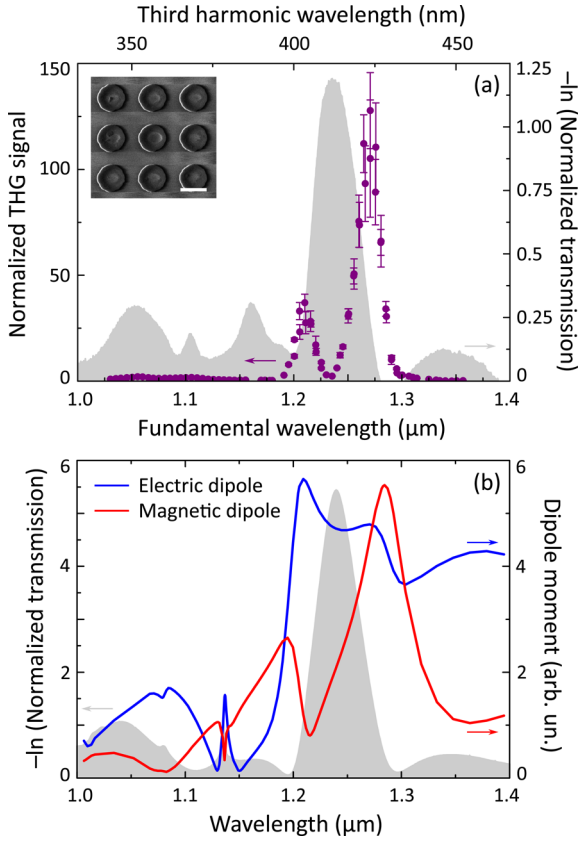


**Figure 3.** (a) THG spectroscopy of Si nanodisk arrays. The negative logarithm of the normalized transmission spectrum of the sample with $p$ = 0.8 $\mu$m, $h$ = 220 nm, and $d$ = 0.5 $\mu$m is given with the gray area indicating a resonance at 1.24 $\mu$m. The THG spectrum of the sample normalized over the spectrum of the substrate is shown in purple dots to be strongly enhanced within the spectral band of the resonance. The inset shows the SEM image of the sample fragment. The scale bar is 500 nm. (b) The simulated transmission spectrum of the fundamental wavelength through the disk array and substrate, showing good agreement with the observed transmission in the experiment. The overlaid blue and red curves give the magnitude of the electric and magnetic dipole moments (respectively) induced in a single disk in the transmission simulation. These dipole moments demonstrate that the electric and magnetic resonances are either side of the observed transmission resonance. The two-peak structure of each dipole moment spectrum contributes to the two-peak THG spectrum in (a).

moments of an individual disk by integrating the induced currents according to the standard expressions for the dipole moments.[18] These dipole moments represent the main multipole moments of the system as seen in the reconstructed transmission spectra (see Supporting Information, Section VI). As follows from Figure 3b, the electric and magnetic resonances are in fact either side of the main resonance observed in transmission, respectively. This stems from the fact that the electric resonance of the sparse nanodisk array undergoes considerable red shift upon decreasing the period of the array and comes to a partial overlap in with the magnetic resonance. The locations of the resulting two resonances notably correspond to the peaks of the observed TH signal as could be expected.

The nanodisks demonstrate a remarkable resonant THG conversion efficiency. To estimate the efficiency, we first calibrate the PMT output by measuring the TH beam directly with a calibrated photodiode power meter (see Supporting


dx.doi.org/10.1021/nl503029j | Nano Lett. 2014, 14, 6488−6492

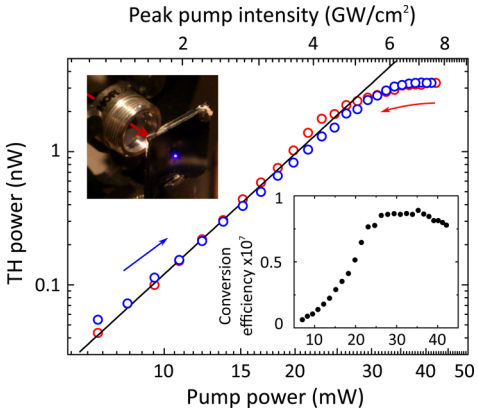


**Figure 4.** Power dependence and conversion efficiency of the resonant THG process in Si nanodisks. Blue circles denote the THG power dependence upon increasing the power of the pump, while red circles denote the reverse procedure both obtained at $\lambda$ = 1.26 $\mu$m fundamental wavelength. The reversibility of the process, as well as the deviation at 5 GW/cm$^2$ pump peak intensity from the cubic dependence given by the black line are demonstrated. The left inset shows a photographic image of the sample irradiated with the invisible IR beam impinging from the back side of the sample as indicated by the red arrow. The blue point represents the scattered TH signal detected by the camera. Note the colors are not reproduced reliably. The right inset shows the conversion efficiency of the nanodisk sample as a function of the pump power.

Information, Section IV). The maximum time-averaged yield of the TH radiation from the disks at $\lambda$ = 420 nm is measured to be $P_{3\omega} \approx 4$ nW, which is observed by naked eye; see the corresponding inset of Figure 4. As proved by measuring a reversible $P_{3\omega}(P_\omega)$ dependence shown in Figure 4, the sample does not undergo irreversible changes even after being irradiated with high-power resonant laser pulses, making it a more attractive tool for the wavelength conversion than any highly absorbing surface plasmon-enhanced media reported thus far.[6,8,19−21] Here, up until the pump power of $P_\omega$ = 30 mW (peak intensity ≈ 5.5 GW/cm$^2$), the dependence represents the expected cubic law, whereas for the higher pump power values the dependence comes to a saturation regime, which is discussed below. The maximum efficiency of IR-to-visible conversion is calculated as $\eta = P_{3\omega}/P_\omega$ and is estimated to peak at $\eta \approx 10^{-7}$. To compare to the previously known record in silicon set by the slow light in photonic crystal waveguides,[22] the nanodisks provide similar conversion rate being essentially a subwavelength device. This improvement can be explained by both higher $\chi^{(3)}$ value observed closer to the three-photon direct transition wavelength at $3\hbar\omega$ = 3.45 eV and lower two-photon absorption build-up sensitivity threshold: in our system the critical peak intensity value is ≈5 GW/cm$^2$, whereas for ref 22, it is 2.5 MW/cm$^2$.

The saturation regime comes as a limitation of using an SOI wafer: at these powers, free carriers generated via two-photon absorption in the bulk Si substrate lead to free-carrier absorption of the pump beam. Using proper expressions[23] and data on two-photon absorption ($\beta$ = 0.5 cm/GW and Im$\chi^{(3)} = 3 \times 10^{-12}$ esu at 1.2 $\mu$m),[24] we calculate the free-carrier absorption attenuation constant to be approximately 10 cm$^{-1}$ at the peak pump intensity of 5 GW/cm$^2$. This corresponds to 1 mm $1/e$ penetration depth of the pump, which is comparable to the thickness of our substrate and could possibly address the observed saturation. We anticipate that by using the reflection geometry or a sample with no underlying Si substrate the threshold intensity of the two-photon absorption effect could be increased by approximately 4 orders of magnitude limited by the thickness of the disks. This could allow for a vast increase of the conversion efficiency; however, note that under these conditions, various limiting factors will start to play a role, such as, for example, the quality of the sample surface and the properties of the environment. Further optimization of the TH yield and output wavelength could be performed by more sophisticated design of the nanoparticles.

In conclusion, using third-harmonic generation microscopy and spectroscopy techniques, we have observed enhanced third-order optical nonlinearities of silicon nanodisks in the vicinity of the magnetic dipolar resonances pumped by femtosecond laser pulses. The efficiency of the IR-to-visible conversion is enhanced by 2 orders of magnitude with respect to the unstructured bulk silicon slab. High conversion efficiency of ≈$10^{-7}$ is found to be limited only by two-photon absorption in the substrate. We believe the results will pave a way to establishing novel efficient platforms of nanoscale resonant nonlinear optical media driven by optically induced magnetic response of low-loss high-index nanoparticles.

## ■ ASSOCIATED CONTENT

### Supporting Information

The detailed information on the used methods and technical results. This material is available free of charge via the Internet at http://pubs.acs.org.

## ■ AUTHOR INFORMATION

### Corresponding Author

*E-mail: shcherbakov@nanolab.phys.msu.ru.

### Notes

The authors declare no competing financial interest.

## ■ ACKNOWLEDGMENTS

The authors would like to thank L. Novotny and H. Giessen for useful comments and suggestions, as well as A. Fedotova for her assistance with the experiment automatization. The authors acknowledge the financial support from Russian Science Foundation (grant #14-12-01144) and Russian Foundation for Basic Research. This work was performed, in part, at the Center for Integrated Nanotechnologies, an Office of Science User Facility operated for the U.S. Department of Energy (DOE) Office of Science. Sandia National Laboratories is a multiprogram laboratory managed and operated by Sandia Corporation, a wholly owned subsidiary of Lockheed Martin Corporation, for the U.S. Department of Energy's National Nuclear Security Administration under contract DE-AC04-94AL85000. The authors also acknowledge a support from the Australian Research Council.

## ■ REFERENCES

(1) Boyd, R. W. *Nonlinear Optics*; Elsevier: New York, 2008.
(2) Kauranen, M.; Zayats, A. V. *Nat. Photonics* **2012**, *6*, 737−748.
(3) Burns, W. K.; Bloembergen, N. *Phys. Rev. B* **1971**, *4*, 3437−3450.
(4) Lippitz, M.; Van Dijk, M. A.; Orrit, M. *Nano Lett.* **2005**, *5*, 799−802.
(5) Hentschel, M.; Utikal, T.; Giessen, H.; Lippitz, M. *Nano Lett.* **2012**, *12*, 3778−3782.
(6) Metzger, B.; Hentschel, M.; Schumacher, T.; Lippitz, M.; Ye, X.; Murray, C. B.; Knabe, B.; Buse, K.; Giessen, H. *Nano Lett.* **2014**, *14*, 2867−2872.

(7) Metzger, B.; Schumacher, T.; Hentschel, M.; Lippitz, M.; Giessen, H. *ACS Photonics* **2014**, *1*, 471−476.
(8) Klein, M. W.; Wegener, M.; Feth, N.; Linden, S. *Opt. Express* **2007**, *15*, 5238−5247.
(9) Kim, E.; Wang, F.; Wu, W.; Yu, Z.; Shen, Y. R. *Phys. Rev. B* **2008**, *78*, 113102.
(10) Reinhold, J.; Shcherbakov, M. R.; Chipouline, A.; Panov, V. I.; Helgert, C.; Paul, T.; Rockstuhl, C.; Lederer, F.; Kley, E.-B.; Tünnermann, A.; Fedyanin, A. A.; Pertsch, T. *Phys. Rev. B* **2012**, *86*, 115401.
(11) Evlyukhin, A. B.; Novikov, S. M.; Zywietz, U.; Eriksen, R. L.; Reinhardt, C.; Bozhevolnyi, S. I.; Chichkov, B. N. *Nano Lett.* **2012**, *12*, 3749−3755.
(12) Kuznetsov, A. I.; Miroshnichenko, A. E.; Fu, Y. H.; Zhang, J.; Luk'yanchuk, B. *Sci. Rep.* **2012**, *2*, 492.
(13) Rose, A.; Huang, D.; Smith, D. R. *Phys. Rev. Lett.* **2013**, *110*, 063901.
(14) Rose, A.; Powell, D. A.; Shadrivov, I. V.; Smith, D. R.; Kivshar, Y. S. *Phys. Rev. B* **2013**, *88*, 195148.
(15) Staude, I.; Miroshnichenko, A. E.; Decker, M.; Fofang, N. T.; Liu, S.; Gonzales, E.; Dominguez, J.; Luk, T. S.; Neshev, D. N.; Brener, I.; Kivshar, Y. *ACS Nano* **2013**, *7*, 7824−7832.
(16) Grahn, P.; Shevchenko, A.; Kaivola, M. *New J. Phys.* **2012**, *14*, 093033.
(17) Liu, S.; Ihlefeld, J. F.; Dominguez, J.; Gonzales, E. F.; Bower, J. E.; Burckel, D. B.; Sinclair, M. B.; Brener, I. *Appl. Phys. Lett.* **2013**, *102*, 161905.
(18) Jackson, J. D. *Classical Electrodynamics*, 3rd ed.; Wiley: New York, 1998.
(19) Liu, T.-M.; Tal, S.-P.; Yu, C.-H.; Wen, Y.-C.; Chu, S.-W.; Chen, L.-J.; Prasad, M. R.; Lin, K.-J.; Sun, C.-K. *Appl. Phys. Lett.* **2006**, *89*, 043122.
(20) Klein, M. W.; Wegener, M.; Feth, N.; Linden, S. *Opt. Express* **2008**, *16*, 8055−8055.
(21) Aouani, H.; Rahmani, M.; Navarro-Cía, M.; Maier, S. A. *Nat. Nanotechnol.* **2014**, *9*, 290−294.
(22) Corcoran, B.; Monat, C.; Grillet, C.; Moss, D. J.; Eggleton, B. J.; White, T. P.; O'Faolain, L.; Krauss, T. F. *Nat. Photonics* **2009**, *3*, 206−210.
(23) McMorrow, D.; Lotshaw, W. T.; Melinger, J. S.; Buchner, S.; Pease, R. L. *IEEE Trans. Nucl. Sci.* **2002**, *49*, 3002−3008.
(24) Lin, Q.; Zhang, J.; Piredda, G.; Boyd, R. W.; Fauchet, P. M.; Agrawal, G. P. *Appl. Phys. Lett.* **2007**, *91*, 021111.